sciendo

POLISH MARITIME RESEARCH 4 (104) 2019 Vol. 26; pp. 16-26
10.2478/pomr-2019-0062

MANOEUVRING PREDICTION OF KVLCC2 WITH HYDRODYNAMIC DERIVATIVES GENERATED BY A VIRTUAL CAPTIVE MODEL TEST

Kun Dai[1]
Yunbo Li[2]
[1] Harbin Engineering University, Harbin, China
[2] College of Ocean Science and Engineering, Shanghai Maritime University, Shanghai, China

ABSTRACT

This paper describes the application of computational fluid dynamics rather than a towing tank test for the prediction of hydrodynamic derivatives using a RANS-based solver. Virtual captive model tests are conducted, including an oblique towing test and circular motion test for a bare model scale KVLCC2 hull, to obtain linear and nonlinear hydrodynamic derivatives in the 3rd-order MMG model. A static drift test is used in a convergence study to verify the numerical accuracy. The computed hydrodynamic forces and derivatives are compared with the available captive model test data, showing good agreement overall. Simulations of standard turning and zigzag manoeuvres are carried out with the computed hydrodynamic derivatives and are compared with available experimental data. The results show an acceptable level of prediction accuracy, indicating that the proposed method is capable of predicting manoeuvring motions.

Keywords: MMG model; KVLCC2; CFD; manoeuvring prediction

INTRODUCTION

Ship manoeuvrability is an important factor affecting the safety of navigation. In order to comply with the manoeuvring standards developed by the International Maritime Organisation [1, 2] in the design process of a ship, a reliable and accurate estimation of the ship's manoeuvrability is required. According to a statement by the Manoeuvring Committee of the International Towing Tank Conference (ITTC, [3]), free running model tests are considered to be the most reliable method for manoeuvrability predictions. Another widely applied method is to simulate manoeuvring motions based on a mathematical model with hydrodynamic derivatives obtained from captive model tests, such as a planar motion mechanism (PMM) test, an oblique towing test (OTT) and a circular motion test (CMT). However, model tests are confined to researchers and ship designers due to the high cost of experiment facilities and difficulties in optimising manoeuvrability at the design phase.

In recent years, the rapidly developing computational fluid dynamics (CFD) technique has been applied in manoeuvring predictions, and can overcome the disadvantages of model tests. There are two classic types of CFD that can be used in predicting ship manoeuvrability. The first is a fully CFD-based approach that simulates standard manoeuvres with a steering rudder and rotating propeller. Mofidi and Carrica [4] presented a direct simulation of a zigzag manoeuvre for the KRISO Container Ship (KCS)in calm water. Shen et al. [5] implemented a dynamic overset grid technique using the open-source code OpenFOAM and presented free-running manoeuvring simulations for a KCS ship in calm water. Wang et al. [6] further extended the direct simulation of a zigzag manoeuvre for an ONR Tumblehome ship in waves, using the same solver as Shen et al. [5]. These direct CFD simulations are believed to give more accurate predictions, since they can resolve complex flows around the hull and its appendages, and can obtain the details of the local flow during manoeuvres. However,

direct CFD simulation is not sufficiently mature for practical applications due to its huge computational cost and the complex numerical techniques required to deal with the coupled motions of the hull, rudder and propeller.

A more practical alternative is known as a system-based method. This performs manoeuvre simulations by solving mathematical models such as the Abkowitz model [7] and the MMG model [8], in which the manoeuvring hydrodynamic derivatives are generated by conducting virtual captive tests using CFD techniques. The CFD method for predicting hydrodynamic derivatives has drawn increasing amounts of attention in the area of manoeuvrability studies over the past few years. Sakamoto et al. [9] conducted unsteady Reynolds averaged Navier-Stokes (URANS)simulations of static and dynamic PMM tests for a bare surface combatant model 5415 using the CFDShip-Iowa code. Guo et al. [10] have conducted circular motion, static drift and heel test simulations for the ONR Tumblehome model using STAR-CCM+, and have investigated manoeuvring motions in calm water with a four-DOF MMG model that considers surge, sway, roll, and yaw. Liu et al. [11] predicted the manoeuvrability of a KCS ship model using the Abkowitz model, with a full set of linear and nonlinear hydrodynamic derivatives determined by virtual captive model tests using STAR-CCM+. Kim et al. [12] and Islam et al. [13] presented PMM simulation results for a KCS model using an open-source RANS solver in OpenFOAM and an in-house code called SHIP_Motion, respectively, and predicted hydrodynamic derivatives from the simulation results.

Regardless of the type of mathematical model used, the reliability of manoeuvring prediction depends on the accuracy of the hydrodynamic derivatives. Although manoeuvring simulations based on CFD have gaining attention lately, it is still difficult to acquire accurate hydrodynamic derivatives using the CFD method. More numerical simulations are needed using CFD for captive model tests and systems-based manoeuvring predictions in order to verify the capability of CFD to predict motion related to ship manoeuvring. In this context, the present study aims to investigate ship manoeuvring motion in the horizontal plane via the application of the MMG model, where the hydrodynamic derivatives are determined by a CFD simulation of the captive model tests. A bare KVLCC2 tanker is selected as the study object. Grid and time step dependency studies are performed for a static drift case to estimate the numerical error and uncertainty due to the grid discretisation and time step. An oblique towing test and a circular motion test are simulated in order to obtain the hydrodynamic derivatives for oblique moving and turning motions. Free manoeuvres such as the turning circle and zigzag tests are simulated with the computed hydrodynamic derivatives, and the simulation results for the manoeuvrability parameters for standard manoeuvres are compared with published data for free-running model tests and EFD-based predictions.

MATHEMATICAL MODEL

COORDINATE SYSTEMS

Two right-handed coordinate systems are used in this paper, as shown in Fig. 1. The trajectory and heading of the ship are defined in o_0–$x_0y_0z_0$, a earth-fixed coordinate system, where the x_0–y_0 plane is fixed on the surface of still water and the z_0 axis points vertically downwards. The hydrodynamic forces acting on the ship are described using a ship-fixed coordinate system *o-xyz*, with the origin taken as the mid-ship position. The *x*-axis points towards the bow, the *y*-axis towards starboard and the *z*-axis vertically downwards. The centre of gravity of the ship is located at (x_G, 0, 0). Ψ is the heading angle, δ is the rudder angle and *r* the yaw rate. *u* and *v* denote the surge velocity and sway velocity, respectively. The drift angle at the mid-ship position is defined by $\beta = \tan^{-1}(-v/u)$, and the total velocity $U = \sqrt{u^2 + v^2}$.

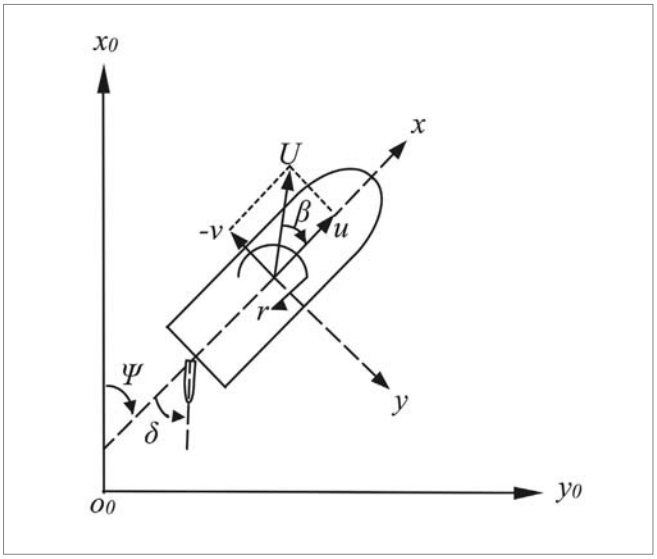

Fig. 1. Coordinate systems used

MOTION EQUATIONS

The 3-DOF (surge, sway and yaw) ship manoeuvring motion can be described by the following equation:

$$\left.\begin{aligned}(m + m_x)\dot{u} - (m + m_y)vr - x_G m r^2 &= X\\ (m + m_y)\dot{v} + (m + m_x)ur + x_G m\dot{r} &= Y\\ (I_{zG} + mx_G^2 + J_z)\dot{r} + x_G m(v + \dot{u}r) &= N\end{aligned}\right\} \quad (1)$$

where *m* is the ship's mass, I_{zG} is the moment of inertia around the centre of gravity. m_x, m_y and J_z are the added masses and added moments of inertia. $\dot{u}$, $\dot{v}$ and $\dot{r}$ are the corresponding surge acceleration, sway acceleration, and yaw acceleration. *X* and *Y* are the corresponding force components, and *N* is the yaw moment.

X, *Y* and *N* on the right-hand side of Eq. (1) are expressed as:

$$\left.\begin{aligned} X &= X_H + X_P + X_R \\ Y &= Y_H + Y_R \\ N &= N_H + N_R \end{aligned}\right\} \quad (2)$$

where the subscripts *H*, *R*, and *P* denote the force and moment due to the hull, rudder, and propeller, respectively.

HULL FORCES

The hydrodynamic forces acting on the hull are expressed as follows, following Yasukawa et al. [8]:

$$\left.\begin{aligned} X_H &= -R_0 + X_{vv}v^2 + X_{vr}vr + X_{rr}r^2 + X_{vvv}v^4 \\ Y_H &= Y_v v + Y_r r + Y_{vvv}v^3 + Y_{vvr}v^2 r + Y_{vrr}vr^2 + Y_{rrr}r^3 \\ N_H &= N_v v + N_r r + N_{vvv}v^3 + N_{vvr}v^2 r + N_{vrr}vr^2 + N_{rrr}r^3 \end{aligned}\right\} \quad (3)$$

where R_0 is the ship's resistance when moving in a straight line, and *X*, *Y*, *N* with subscripts *u*, *v*, *r* are the hydrodynamic derivatives on manoeuvring.

PROPELLER FORCE

The longitudinal force of the propeller X_P is described as follows:

$$X_P = (1 - t_P)\,\rho n_P^2 D_P^4 K_T(J_P) \quad (4)$$

$$K_T(J_P) = k_2 J_P^2 + k_1 J_P + k_0 \quad (5)$$

$$J_P = u(1 - w_P) / (n_P D_P) \quad (6)$$

where t_P is the thrust deduction factor, ρ is the water density, D_P is the diameter of the propeller, and K_T is the thrust coefficient, which can be expressed as a second-order polynomial function of the propeller advance ratio J_P. n_P is the propeller revolution. w_P is the wake coefficient at the propeller position in manoeuvring motion, and according to [8] can be written as:

$$(1 - w_P) / (1 - w_{P0}) = 1 + [1 - \exp(-C_1|\beta_P|)]\,(C_2 - 1) \quad (7)$$

where w_{P0} is the wake coefficient at the propeller position in straight motion, β_P is the geometric inflow angle to propeller in manoeuvring motion, C_1 denotes the wake change characteristic versus β_P and C_2 represents the value of $(1 - w_P)/(1 - w_0)$ at large β_P.

For the purposes of the present simulations, the open water characteristics of the corresponding propeller are approximated based on the open water propeller test of the National Maritime Research Institute, Japan [19]:

$$K_T(J_P) = -0.1385J_P^2 - 0.2753J_P + 0.2931 \quad (8)$$

$$10K_Q(J_P) = -0.2045J_P^2 - 0.1856J_P + 0.3071 \quad (9)$$

RUDDER FORCES

The rudder forces are expressed by a combination of interaction factors and the rudder normal force:

$$\left.\begin{aligned} X_R &= -(1 - t_R)F_N \sin\delta \\ Y_R &= -(1 - a_H)F_N \cos\delta \\ N_R &= -(x_R - a_H x_H)F_N \cos\delta \end{aligned}\right\} \quad (10)$$

where F_N is the rudder normal force. t_R is the steering resistance reduction factor, which defines the reduction in rudder resistance during steering. a_H is the rudder force increase factor, which indicates the additional lateral force acting on the ship by steering. x_R is the longitudinal position of the rudder, while x_H denotes the longitudinal acting point of the additional lateral force component. The rudder normal force is expressed as Eqs. (9)–(12).

$$F_N = \frac{1}{2}\rho A_R (u_R^2 + v_R^2)\frac{6.13\lambda}{\lambda + 2.25}\sin a_R \quad (11)$$

$$a_R = \delta - \tan^{-1}(v_R / u_R) \quad (12)$$

$$v_R = U\gamma_R(\beta - l_R' r') \quad (13)$$

$$u_R = \varepsilon u(1 - w_P)\sqrt{\eta\left[1 + \kappa\left(\sqrt{1 + \frac{8K_T}{\pi J_P^2}} - 1\right)\right]^2 + (1 - \eta)} \quad (14)$$

where A_R is the rudder area, λ is the rudder aspect ratio, u_R and v_R are the longitudinal and lateral rudder inflow velocities induced by propeller rotation, respectively; ε is the ratio of the wake fraction at the rudder position to that at the propeller position, η is introduced to express the percentage of the rudder area in the propeller race, which is evaluated based on the relative propeller-rudder position; κ is the interaction factor between propeller and rudder; *U* is the resultant velocity; γ_R represents the flow straightening coefficients; and l_R is the effective longitudinal coordinate of the rudder position.

It should be noted that in the rest of this paper, symbols with the prime symbol ' represent a non-dimensionalised value. Force and moment are non-dimensionalised by $(1/2)\,\rho L_{pp} dU^2$ and $(1/2)\,\rho L_{pp}^2 dU^2$, respectively, where *d* is the ship draft and L_{pp} is the length of the ship between perpendiculars. The mass and moment of inertia are non-dimensionalised by $(1/2)\rho L_{pp}^2 d$ and $(1/2)\rho L_{pp}^4 d$, respectively. Lateral velocity *v* and yaw rate *r* are made non-dimensional as follows:

$$v' = v/U \qquad r' = rL_{pp}/U \quad (15)$$

Fig. 2. Geometry of the KVLCC2 tanker

MODEL SHIP DESCRIPTION

The sample ship studied here is the bare KVLCC2 tanker model. This ship is a very popular test model, and many experimental and CFD test results for this model are open to the public and have been discussed in workshops and conferences [14–16]. Table 1 shows the main particulars. In the table, the parameters of ship models with lengths 2.909 m (L-3 model) and 7.00 m (L-7 model) are shown together with those of a full-scale ship. In this paper, the L-3 model is used for simulation of the captive model tests, while the L-7 model is used for prediction of manoeuvring motions. The geometry of the KVLCC2 tanker is shown in Fig. 2.

Tab. 1. Main particulars of KVLCC2

	Full scale	L-3 model	L-7 model
Scale	1.00	1/110	1/45.7
L_{pp} (m)	320.0	2.909	7.00
B (m)	58.0	0.527	1.27
D (m)	20.8	0.189	0.46
∇(m3)	312,622	0.235	3.27
x_G (m)	11.2	0.102	0.25
C_b	0.810	0.810	0.810
Propeller type	FP	FP	FP
D_P	9.86	0.090	0.216
Rudder type	Horn	Horn	Horn
H_R	15.8	0.144	0.345
A_R	112.5	0.00928	0.0539

NUMERICAL METHOD

In this study, the CFD software STAR-CCM+ is used in the numerical simulations. This code solves closed RANS equations using the isotropic blended SST k-ω turbulence model. The flow domain is discretised using the finite volume method (FVM). The temporal terms are performed with a first-order backwards Euler scheme, and the convection and term diffusion are discretised with a second-order upwind scheme and a second-order scheme, respectively. The pressure-velocity coupling is solved using a SIMPLE algorithm. An all-y+ treatment is employed for near-wall modelling, which is a hybrid treatment emulating a high y+ wall treatment with a coarse mesh and low y+ wall treatment with a fine mesh. The free surface is captured by the two-phase volume of fluid (VOF) technique. In our numerical simulations, three degrees of freedom are considered: surge, sway and raw. A rotation and translation module is adopted for the simulation of captive model tests in calm and deep water conditions.

COMPUTATIONAL CASES

In order to obtain the linear and nonlinear hydrodynamic derivatives in the third-order MMG model in Equations (3), simulations of an oblique towing test and a circular motion test are carried out for the KVLCC2 model (L-3 model) without a propeller or rudder. Table 2 presents a summary of the computational conditions. All simulations are performed under static conditions in which all ship motions are restricted. The calculations are conducted on two DELL local workstations (Intel Xeon E5-2670v3 @2.3 GHz, 32 GB) using six processors. The simulations are run for up to 30 s (simulation time) to attain a stable output. The ship speed U is set to Fr = 0.142. The Froude number is defined as $Fr = U / (gL_{pp})^{1/2}$, where g is the gravitational acceleration.

Tab. 2. Computational cases for OTT and CMT

Test	Fr	r'	β(°)
OTT	0.142	0	0, ±2, ±4, ±6, ±8, ±12, ±16
CMT	0.142	0.2,0.6,0.8	0, ±2, ±4, ±6, ±8, ±12, ±16

COMPUTATIONAL DOMAIN AND GRID

An overview of the computational grid and boundary conditions is shown in Figure 3. The inlet is placed at $1.0L_{pp}$ in front of the bow, the outlet $3.0L_{pp}$ behind the stern, the top $0.5L_{pp}$ above the free surface, the bottom $1.5L_{pp}$ below the still free surface, and each lateral boundary $1.5L_{pp}$ away from starboard and port sides, respectively. As for the boundary conditions, the outlet plane is specified as pressure outlet, the hull surface is treated as non-slip wall, and the rest of the boundaries are specified as velocity inlet. Wave damping is applied at the outlet and side walls to reduce wave oscillations.

The computational domain is discretised using an unstructured hexahedral grid. In order to capture the flow and wave features during the motion of the ship, the grid around the ship and free surface is refined, as shown in Fig. 3. On the surfaces of the hull, prismatic cells are used to achieve better resolution of the flow near the boundary, and the value

of y+ is around 40 along the hull. Refinement of the grid near the bow and stern of the hull is employed to resolve the flow, as shown in Fig. 4.

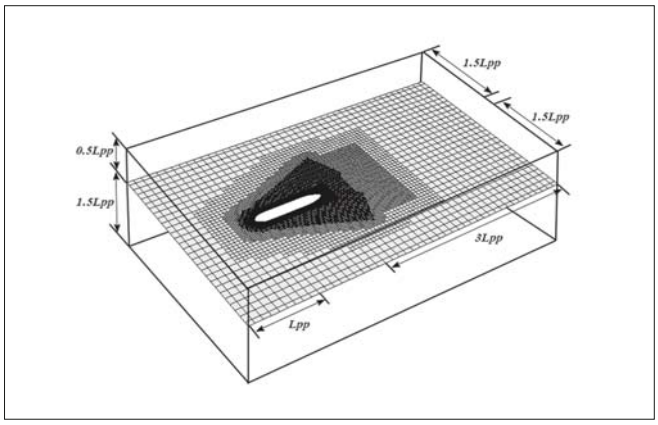

Fig. 3. CFD computational domain and boundary conditions

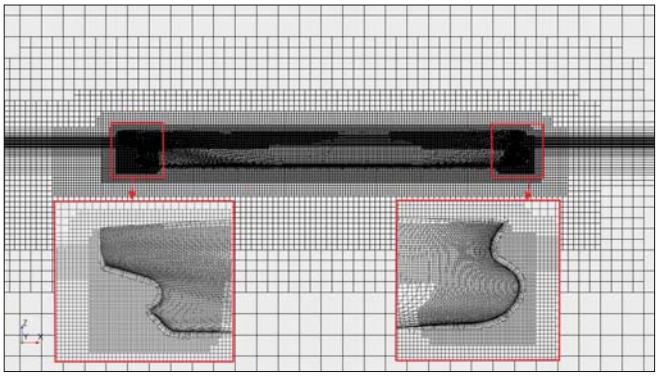

Fig. 4. Grid structure in the regions around the ship

CONVERGENCE STUDY

Grid size and time step convergence studies are performed for a static drift case with $\beta = 12°$ at $Fr = 0.142$, in order to evaluate the discretisation errors caused by the grid size and time step. A verification study is conducted following the methodology discussed by Stern et al. [17] and Wilson et al. [18].

In the grid spacing convergence study, all grid parameters are given as a percentage of the base size, so that the grid can be refined systematically. A refinement ratio of $r_G = \sqrt{2}$ is applied for grid refinement. Three sets of grids, referred to here as coarse (S3), medium (S2), and fine (S1), were generated based on a refinement ratio consisting of 1.07 M, 2.38 M and 5.66 M cells, respectively. The time step for the coarse, medium and fine grids was 0.03 s and the computing time was about 10, 24 and 60 hours, respectively. In the time step convergence study, the simulation was performed with a medium grid. Three sets of time steps, referred to here as 0.0424 s (S3), 0.03 s (S2), and 0.0212 s (S1), were used based on the refinement ratio $r_T = \sqrt{2}$. The computing times for the coarse, medium and fine time step were about 16, 24 and 31 hours, respectively. The results of the grid convergence and time step convergence studies for simulation of the static drift case are shown in Tables 3 and 4, respectively. It can be observed from Table 3 that X', Y' and N' all achieve monotonic convergence with $0 < R_G < 1$ in the grid convergence study. Similarly, X', Y' and N' all achieve monotonic convergence with $0 < R_T < 1$ in the time step convergence study, as shown in Table 4. Thus, a medium coarse grid with 2.38 M cells and a medium time step of 0.03 s are used in subsequent simulations, in order to balance the computation cost and accuracy.

Tab. 3. Grid convergence of OTT simulation with β =12°

Grid	ID	Grid Size	X'	Y'	N'
Fine	S1	5.66M	−0.02307	0.06952	0.02654
Medium	S2	2.38 M	−0.02309	0.07044	0.02673
Coarse	S3	1.07 M	−0.02333	0.07162	0.02694
RG			0.05674	0.77551	0.92031
PG			8.27886	0.73357	0.23961
UG (%S2)			0.11760	10.89307	23.81957
UGC (%S2)			0.05698	3.19688	7.69665
Convergence			Monotonic	Monotonic	Monotonic

Tab. 4. Time step convergence for the OTT simulation with β =12°

Time−step	ID	Time−step Size	X'	Y'	N'
Fine	S1	0.0212 s	−0.02294	0.07048	0.02688
Medium	S2	0.03 s	−0.02309	0.07044	0.02673
Coarse	S3	0.0424 s	−0.02337	0.07000	0.02655
RT			0.51528	0.08840	0.79220
PT			1.9131	6.9996	0.6721
UT (%S2)			2.3672	0.2606	3.6208
UTC (%S2)			0.8494	0.1277	0.7660
Convergence			Monotonic	Monotonic	Monotonic

NUMERICAL RESULTS

FORCES AND MOMENTS

The computed hydrodynamic forces and moments from the simulations of CMT and OTT are compared with EFD data from Yasukawa et al. [8], as plotted in Figs. 5–8. It should be noted that the inertia forces are subtracted from the EFD data. As shown in Fig. 5, the numerical and computational results are in good agreement with the experimental data, although some discrepancies between CFD and EFD can be found at larger drift angles, which are likely to be due to

severe flow separation around the hull. From Figs. 6–8, it can be seen that discrepancies between CFD and EFD become more significant as the yaw rate increases. In general, CFD computation underestimates the sway force but overestimates the yaw moment. Moreover, significant deviation occurs at larger negative drift angles under conditions of $r' = 0.8$. These discrepancies may be caused by the restriction of ship motion to a large extent.

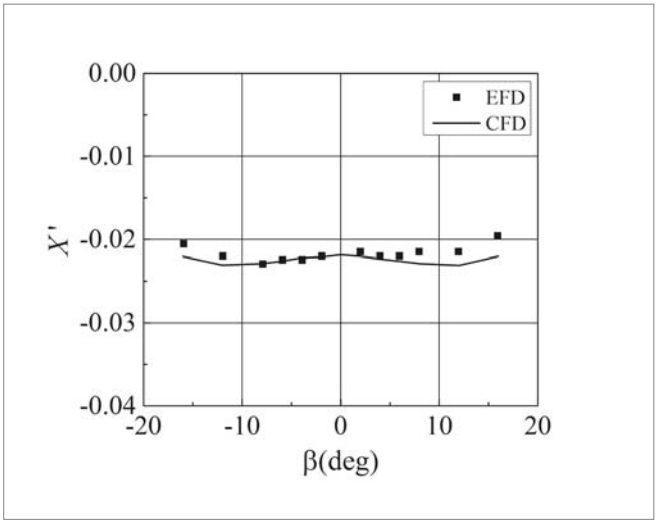

(a1)

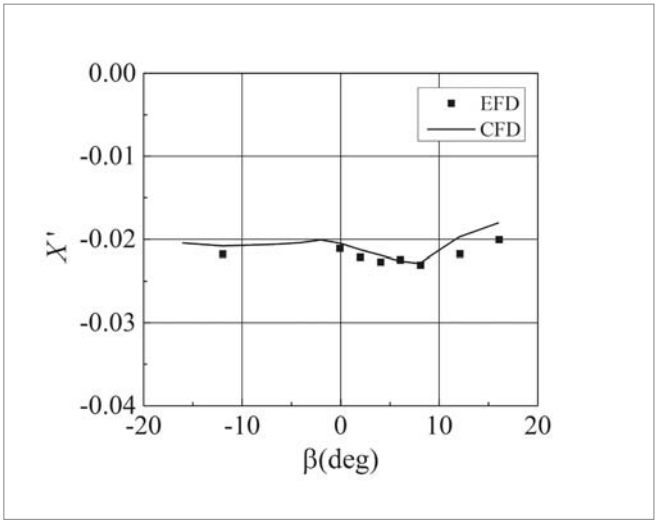

(a2)

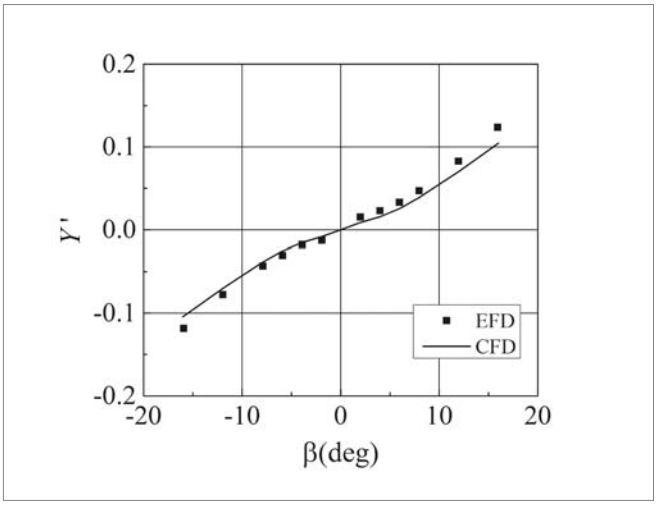

(b1)

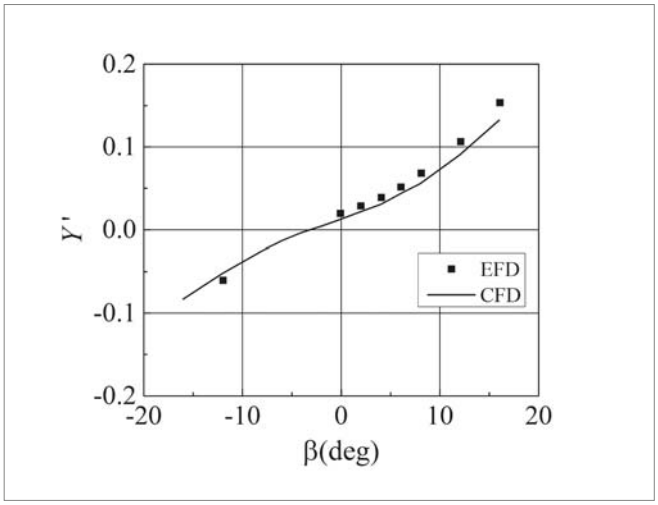

(b2)

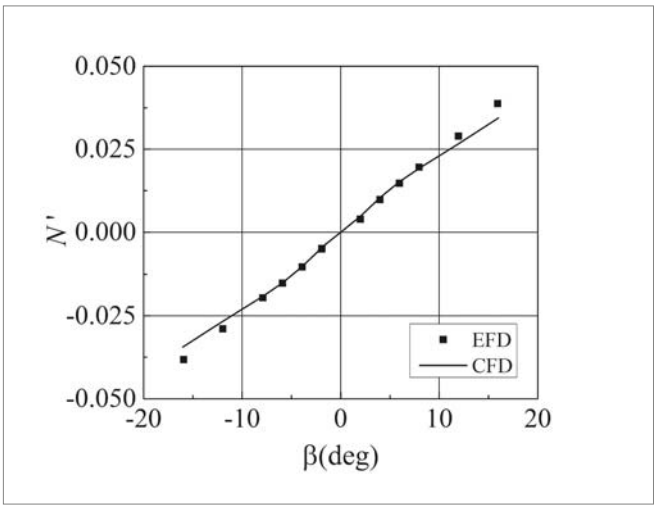

(c1)

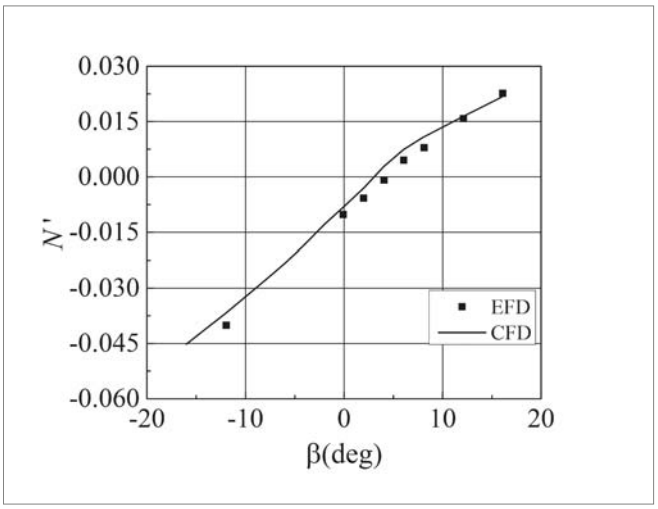

(c2)

Fig. 5. Comparison of results for OTT: (a1)X'; (b1)Y'; (c1)N'

Fig. 6. Comparison of results for CMT AT at r'=0.2: (a2)X'; (b2)Y'; (c2)N'

HYDRODYNAMIC DERIVATIVES

As shown in Eq. (1), the hydrodynamic forces and moment can be expressed by a series of polynomials. The dimensionless hydrodynamic derivatives are determined from the CFD data for captive CMT and OTT, using a least squares method. Fig. 9 presents a comparison of the hydrodynamic derivatives obtained from the EFD and CFD

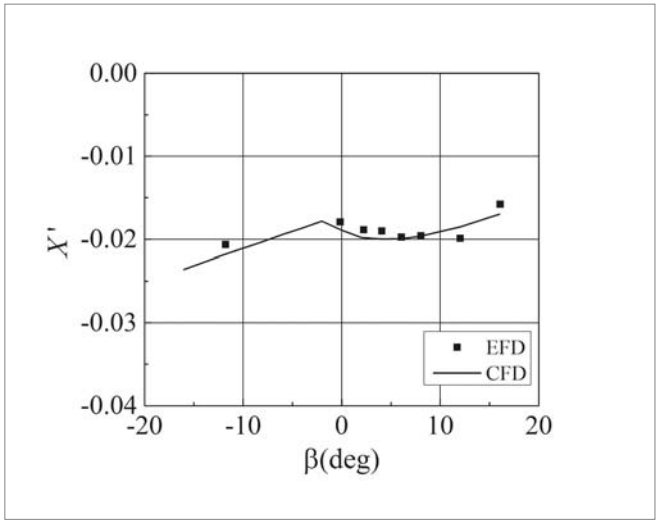

(a3)

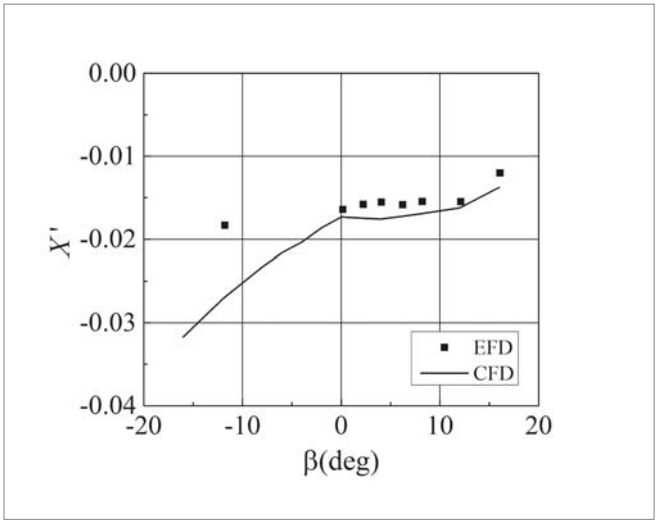

(a4)

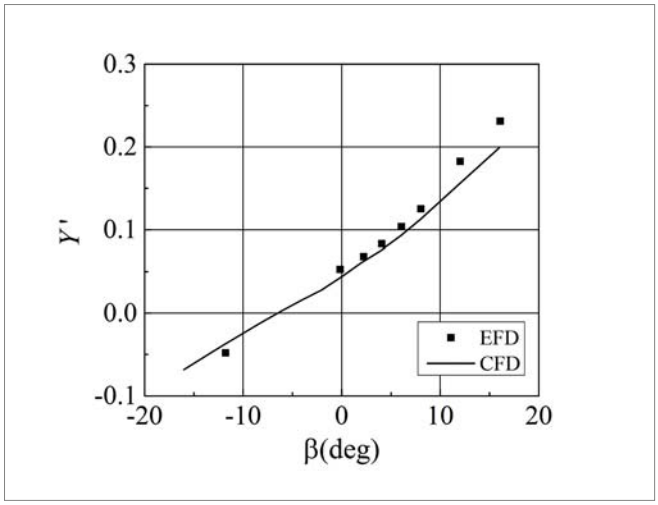

(b3)

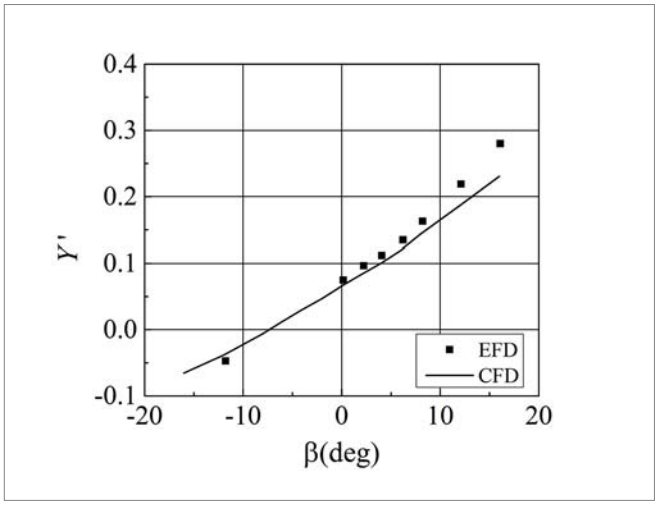

(b4)

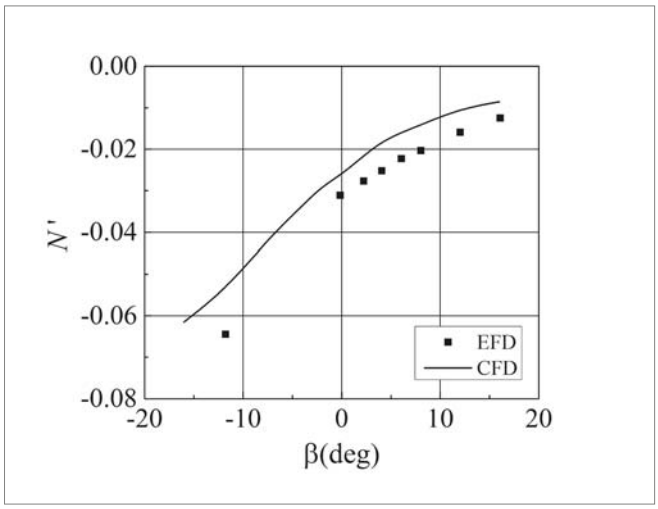

(c3)

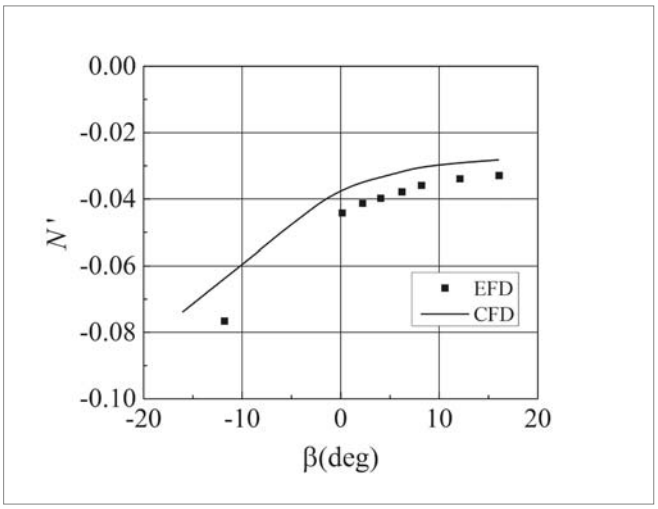

(c4)

Fig. 7. Comparison of results for CMT at r'=0.6: (a3)X'; (b3)Y'; (c3)N'

Fig. 8. Comparison of results for CMT at r'=0.8: (a4)X'; (b4)Y'; (c4)N'

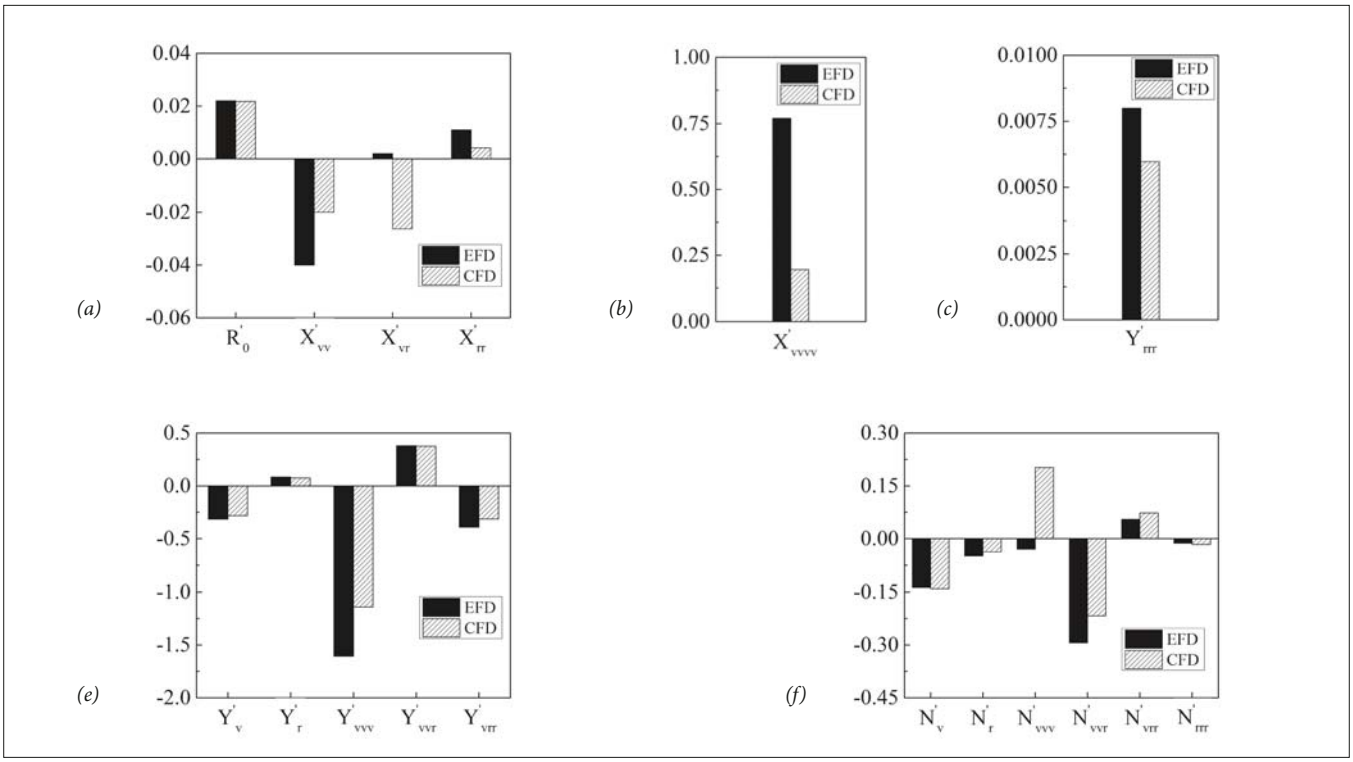

Fig. 9. Comparison of hydrodynamic derivatives

results, where the EFD results are obtained from Yasukawa et al. [8]. The derivatives of X'_{vv}, X'_{vr}, X'_{rr}, X'_{vvvv} obtained by CFD computation show significant deviations from the EFD results. However, the surge force is much less important to the trajectory in manoeuvres as compared with the sway force and yaw moment, meaning that these deviations may have a negligible impact on the manoeuvring simulations. The derivatives of Y and N from CFD show good agreement with those from EFD, except for Y'_{vvv}, Y'_{rrr}, N'_{vvv}, and N'_{rrr}, indicating that this may result in errors in the sway force and yaw moment in manoeuvring simulations.

SIMULATION OF STANDARD MANOEUVRES

A turning circle test and zigzag test simulations are carried out for the L-7 model using the derivatives obtained from the CFD data, and are compared with the results of a free-running model test (FRMT) from MARIN [16] and predictions by Yasukawa et al. [8] using derivatives obtained from a captive model test. The inertia terms and parameters for the modules of the propeller and rudder obtained from model tests are listed in Table 5, and are taken from Yasukawa et al. [8]. The trajectory for a turning circle test for $\delta = \pm 35°$ is presented in Fig. 10. The time histories of the heading angle and rudder angle for ±10°/±10° and ±20°/±20° zigzag manoeuvres are plotted in Fig. 11. A comparison of the manoeuvring parameters of advance (A_D), tactical diameter (D_T) and overshoot angles (OSAs) is presented in Table 6, and gives a relative comparison error E (%) defined as (1-Cal./FRMT)×100%, where 'Cal.' denotes the parameters predicted by the present method and taken from Yasukawa et al. [8].

As shown in Fig. 10, the trajectory of the turning test matches well in both simulations, although the parameters of advance and tactical diameter are under-predicted by the proposed method and over-predicted by Yasukawa et al. The simulation results of Yasukawa et al. show better accuracy, with a maximum value 5.8% larger than the test results, while the turning indices calculated by the proposed method have a maximum value 9.28% than the EFD data. From Fig. 11, it can be seen that both simulation results roughly agree with the test data and capture the overall trend of the zigzag manoeuvres. In Table 6, a comparison of the errors in the OSAs from a captive model test-based method are positive, except for the second OSA, indicating that Yasukawa et al. under-predict the first and second OSAs compared with FRMT. In contrast, the proposed method over-predicts the OSAs, resulting in negative comparison errors as shown in Table 6. Generally speaking, the captive model test-based method gives worse predictions for zigzag manoeuvres than the proposed method.

Tab. 5. Parameters used in the simulation

m'_x	0.022	t_R	0.387	C_1	2.0
m'_y	0.223	l'_R	−0.710	$C_2\ (\beta_p > 0)$	1.6
J'_z	0.011	w_{P0}	0.40	$C_2\ (\beta_p > 0)$	1.1
t_P	0.220	ε	1.09	$\gamma_R\ (\beta_R > 0)$	0.395
a_H	0.312	κ	0.50	$\gamma_R\ (\beta_R > 0)$	0.640
x'_H	−0.464	λ	2.747		

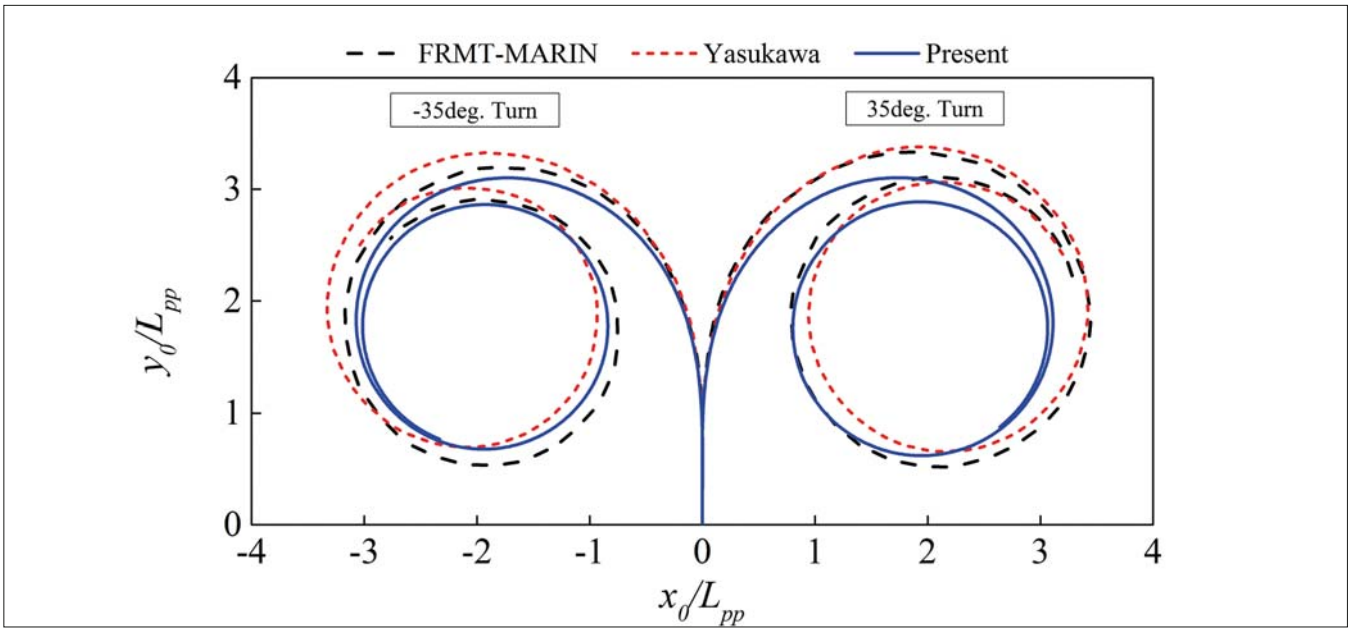

Fig. 10. Comparison of turning trajectory (δ = ±35°)

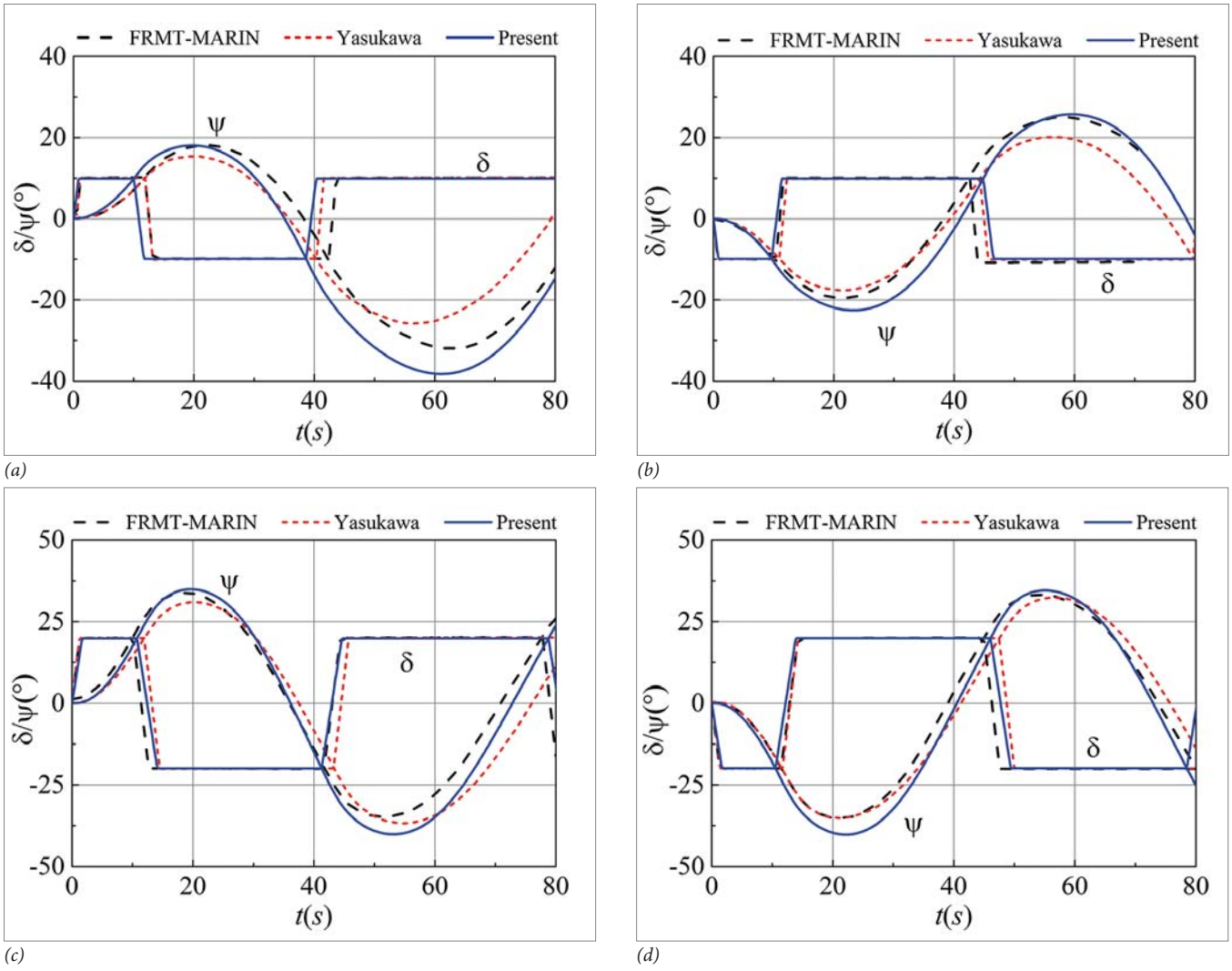

Fig. 11. Comparison of time histories of the heading angle and rudder angle in zigzag manoeuvres: (a) 10°/10° zigzag; (b) –10°/–10° zigzag; (c) 20°/20° zigzag; (d) –20°/–20° zigzag

Tab. 6. Comparison of manoeuvring parameters

Manoeuvres	Parameters	FRMT-MARIN	Yasukawa	E(%)	Present	E(%)
+35° Turn	$A_D\,(L_{pp})$	3.25	3.31	–1.85	3.02	7.08
	$D_T\,(L_{pp})$	3.34	3.36	–0.60	3.03	9.28
–35° Turn	$A_D\,(L_{pp})$	3.11	3.26	–4.82	3.02	2.89
	$D_T\,(L_{pp})$	3.08	3.26	–5.84	2.98	3.25
10°/10°	1st OSA (°)	8.2	5.2	36.59	8.3	–1.22
	2nd OSA (°)	21.9	15.8	27.85	28.30	–29.22
–10°/–10°	1st OSA (°)	9.5	7.6	20.00	12.60	–32.63
	2nd OSA (°)	15.0	10.2	32.00	15.7	–4.67
20°/20°	1st OSA (°)	13.7	10.9	20.44	15.3	–11.68
	2nd OSA (°)	14.8	16.8	–13.51	20.2	–36.49
–20°/–20°	1st OSA (°)	15.1	14.5	3.97	20.3	–34.44
	2nd OSA (°)	13.2	12.4	6.061	14.6	–10.61

CONCLUSION

In this study, CFD-based prediction of 3-DOF ship manoeuvring is implemented for the KVLCC2 model, where the hydrodynamic derivatives of the hull in the 3-DOF MMG model are determined by simulation of a circular motion test and an oblique towing test using CFD. A convergence study is carried out for the simulation of a static drift case. The computed force and moment are validated by comparison with available experimental data. The hydrodynamic derivatives are determined from the computed forces and moments and compared with those from published experimental data, and show satisfactory agreement with experiment except for some high-order terms.

A turning circle test and zigzag manoeuvres are simulated using the computed hydrodynamic derivatives. The numerical results are compared with data from free running model tests and predictions based on a captive model test. From these comparisons, it can be concluded that although prediction based on captive model test shows better performance overall, the present method is effective in determining the hydrodynamic derivatives in the MMG model and predicting ship manoeuvrability.

ACKNOWLEDGMENT

This work was supported by the National Natural Science Foundation of China (Grant Nos. 51979157) and the Natural Science Foundation of Shanghai, China. (Grant Nos. 19ZR1422500).

REFERENCES

1. IMO Res MSC (2002): *Standards for Ship Manoeuvrability*, 137 (76).
2. IMO MSC/Circ.1053 (2002): *Explanatory Notes to the Standards for Ship Manoeuvrability.*
3. ITTC, Manoeuvring Committee (2008): *Final Report and Recommendations to the 25th ITTC*. Proceedings of 25th International Towing Tank Conference, Fukuoka, Japan.
4. Mofidi A., Carrica P.M. (2014): *Simulations of Zigzag Maneuvers for a Container Ship with Direct Moving Rudder and Propeller*. Comput. Fluids, 96, 191–203.
5. Shen Z., Wan D., Carrica P.M. (2015): *Dynamic Overset Grids in OpenFOAM with Application to KCS Self-Propulsion and Maneuvering*. Ocean. Eng., 108, 287–306.
6. Wang J., Zou L., Wan D. (2018): *Numerical Simulations of Zigzag Maneuver of Free Running Ship in Waves by RANS-Overset Grid Method*. Ocean. Eng., 162, 55–79.
7. Abkowitz, M.A. (1964): *Lectures on Ship Hydrodynamics-Steering and Manoeuvrability.* In: Hydro- and Aerodynamics Lab, Report No. Hy-5, Lyngby, Copenhagen, Denmark.
8. Yasukawa H., Yoshimura, Y. (2015): *Introduction of MMG Standard Method for Ship Maneuvering Predictions*. Journal of Marine Science and Technology, 20(1), 37–52.
9. Sakamoto N., Carrica P.M., Stern F. (2012): *URANS Simulations of Static and Dynamic Maneuvering for Surface Combatant: Part 1. Verification and Validation for Forces, Moment, and Hydrodynamic Derivatives*. Journal of Marine Science and Technology, 17(4), 422–445.

10. Hai-peng G., Zao-jian Z. (2017): *System-Based Investigation on 4-DOF Ship Maneuvering with Hydrodynamic Derivatives Determined by RANS Simulation of Captive Model Tests*. Applied Ocean Research, 68, 11-25.

11. Yi L., Lu Z., Zaojian Z., Haipeng G. (2018): *Predictions of Ship Maneuverability Based on Virtual Captive Model Tests*. Engineering Applications of Computational Fluid Mechanics, 12(1), 334–353.

12. Kim H., Akimoto H., Islam H. (2015): *Estimation of the Hydrodynamic Derivatives by RANS Simulation of Planar Motion Mechanism Test*. Ocean Engineering, 108, 129–139.

13. Islam H., Guedes Soares C. (2018): *Estimation of Hydrodynamic Derivatives of a Container Ship Using PMM Simulation in OpenFOAM*. Ocean Engineering, 108, 164–425.

14. Ueno M., Yoshimura Y., Tsukada Y., Miyazaki H. (2009): *Circular Motion Tests and Uncertainty Analysis for Ship Maneuverability*. Journal of Marine Science and Technology, 14, 469–484.

15. Yoshimura Y., Ueno M., Tsukada Y. (2008): *Analysis of Steady Hydrodynamic Force Components and Prediction of Manoeuvring Ship Motion with KVLCC1, KVLCC2 and KCS*. SIMMAN 2008, Workshop on verification and validation of ship manoeuvring simulation method, Workshop Proceedings, Vol. 1, Copenhagen, pp. E80–E86.

16. SIMMAN (2008): *Part C Captive and Free Model Test Data*. Workshop on verification and validation of ship manoeuvring simulation method, Workshop Proceedings, Vol. 1, Copenhagen.

17. Stern F., Wilson R.V., Coleman H.W., Paterson E.G. (2001): *Comprehensive Approach to Verification and Validation of CFD Simulations Part 1: Methodology and Procedures*. Journal of Fluids Engineering, 123(4), 793–802.

18. Wilson R., Shao J., Stern F. (2004): *Discussion: Criticisms of the "Correction Factor" Verification Method*. Journal of Fluids Engineering, 126(4), 704–706.

19. SIMMAN (2014). Retrieved from http://simman2014.dk/ship-data/moeri-kvlcc2-tanker/geometry-and-conditions-moeri-kvlcc2-tanker/.

CONTACT WITH THE AUTHORS

Kun Dai
e-mail: kundai@hrbeu.edu.cn

College of Shipbuilding Engineering
Harbin Engineering University, Harbin
China

Yunbo Li
e-mail: multihull@163.com

College of Ocean Science and Engineering
Shanghai Maritime University, Shanghai
China